Vol. 39 (2008) ACTA PHYSICA POLONICA B No 9

GLUON SATURATION FROM DIS TO NUCLEUS–NUCLEUS COLLISIONS*

François Gelis

CERN, PH-TH
Case C01600, CERN
CH-1211 Geneva 23, Switzerland

(Received May 12, 2008)

In this series of three lectures, I discuss several aspects of high energy scattering among hadrons in Quantum Chromodynamics. The first lecture is devoted to a presentation of gluon saturation and of the Color Glass Condensate (CGC). The second lecture describes the application of this framework to Deep Inelastic Scattering and to proton–nucleus collisions. In the third lecture, we present the application of the CGC to the study of high energy hadronic collisions, with emphasis on nucleus–nucleus collisions. In particular, we provide the outline of a proof of high energy factorization for inclusive gluon production.

PACS numbers: 11.15.Kc, 11.80.La, 12.38.–t

1. Introduction

Quantum Chromodynamics (QCD) is very successful at describing hadronic scatterings involving very large momentum transfers. A crucial element in these successes is the asymptotic freedom of QCD [1], that renders the coupling weaker as the momentum transfer scale increases, thereby making perturbation theory more and more accurate. The other important property of QCD when comparing key theoretical predictions to experimental measurements is the factorization of the short distance physics which can be computed reliably in perturbation theory from the long distance strong coupling physics related to confinement. The latter are organized into non-perturbative parton distributions, that depend on the scales of time and transverse space at which the hadron is resolved in the process under consideration. In fact, QCD not only enables one to compute the perturbative

* Presented at the School on QCD, Low-x Physics, Saturation and Diffraction, Copanello, Calabria, Italy, July 1–14, 2007.

hard cross-section, but also predicts the scale dependence of the parton distributions. A generic issue in the application of perturbative QCD to the study of hadronic scatterings is the occurrence of logarithmic corrections in higher orders of the perturbative expansion. These logarithms can be large

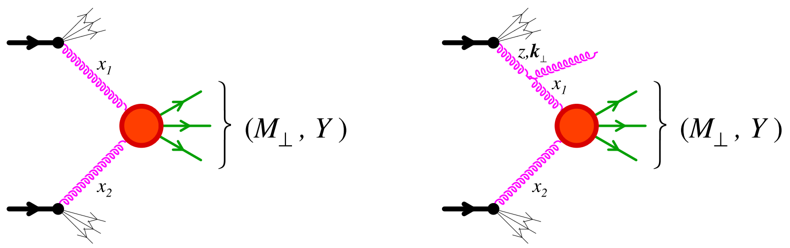

Fig. 1. Generic hard process in the scattering of two hadrons. Left: Leading Order. Right: Next-to-Leading Order correction involving gluon radiation in the initial state.

enough to compensate the extra coupling constant $\alpha_{\rm s}$ they come accompanied with, thus voiding the naive, fixed order, application of perturbation theory. Consider for instance a generic gluon–gluon fusion process, as illustrated on the left of figure 1, producing a final state of momentum P^μ. The two gluons have longitudinal momentum fractions $x_{1,2}$ given by

$$x_{1,2} = \frac{M_\perp}{\sqrt{s}}\, e^{\pm Y}\,, \tag{1}$$

where $M_\perp \equiv \sqrt{\boldsymbol{P}_\perp^2 + P^2}$ ($P^2 \equiv P_\mu P^\mu$ is the invariant mass of the final state) and $Y \equiv \ln(P^+/P^-)/2$. On the right of figure 1 is represented a radiative correction to this process, where a gluon is emitted from one of the incoming lines. Roughly speaking, such a correction is accompanied by a factor

$$\alpha_{\rm s} \int_{x_1} \frac{dz}{z} \int^{M_\perp} \frac{d^2\boldsymbol{k}_\perp}{k_\perp^2}\,, \tag{2}$$

where z is the momentum fraction of the gluon before the splitting, and $\boldsymbol{k}_\perp$ its transverse momentum. Such corrections produce logarithms, $\log(1/x_1)$ and $\log(M_\perp)$, that respectively become large when x_1 is small or when $M_\perp$ is large compared to typical hadronic mass scales. These logarithms tell us that parton distributions must depend on the momentum fraction x and on a transverse resolution scale $M_\perp$, that are set by the process under consideration. In the linear regime[1], there are "factorization theorems" —

[1] We use the denomination "linear" here to distinguish it from the saturation regime discussed later that is characterized by non-linear evolution equations.

k_t-*factorization* [2] in the first case and *collinear factorization* [3] in the second case — that tell us that the logarithms are universal and can be systematically absorbed in the definition of parton distributions[2]. The x dependence that results from resumming the logarithms of $1/x$ is taken into account by the BFKL equation [4]. Similarly, the dependence on the transverse resolution scale $M_\perp$ is accounted for by the DGLAP equation [5].

The application of QCD is a lot less straightforward for scattering at very large center of mass energy, and moderate momentum transfers. This kinematics in fact dominates the bulk of the cross-section at collider energies. A striking example of this kinematics is encountered in Heavy Ion Collisions (HIC), when one attempts to calculate the multiplicity of produced particles. There, despite the very large center of mass energy[3], typical momentum transfers are small[4], of the order of a few GeVs at most. In this kinematics, two phenomena that become dominant are

- **Gluon saturation**: linear evolution equations (DGLAP or BFKL) for the parton distributions implicitly assume that the parton densities in the hadron are small and that the only important processes are splittings. However, at low values of x, the gluon density may become so large that gluon recombinations are an important effect.

- **Multiple scatterings**: processes involving more than one parton from a given projectile become sizeable.

It is highly non trivial that this dominant regime of hadronic interactions is amenable to a controlled perturbative treatment within QCD, and the realization of this possibility is a major theoretical advance in the last decade. The goal of these three lectures is to present the framework in which such calculations can be carried out.

In the first lecture, we will address the evolution of the parton model to small values of the momentum fraction x and the saturation of the gluon distribution. After a qualitative description of the partonic structure of a hadron at high energy, we will discuss the phenomenon of parton saturation at small x.

In the second lecture, after illustrating the tremendous simplification of high energy scattering in the eikonal limit, we will derive the BFKL equation and its non-linear extension, the BK equation. We end the lecture with

[2] The latter is currently more rigorously established than the former.

[3] At RHIC, center of mass energies range up to $\sqrt{s} = 200$ GeV/nucleon; the LHC will collide nuclei at $\sqrt{s} = 5.5$ TeV/nucleon.

[4] For instance, in a collision at $\sqrt{s} = 200$ GeV between gold nuclei at RHIC, 99% of the multiplicity comes from hadrons whose $p_\perp$ is below 2 GeV.

a discussion of the close analogy between the energy dependence of scattering amplitudes in QCD and the temporal evolution of reaction–diffusion processes in statistical mechanics.

The third lecture is devoted to the study of nucleus–nucleus collisions at high energy. Our main focus is the study of bulk particle production in these reactions within the CGC framework. After an exposition of the power counting rules in the saturated regime, we explain how to keep track of the infinite sets of diagrams that contribute to the inclusive gluon spectrum. Specifically, we demonstrate how these can be resummed at leading and next-to-leading order by solving classical equations of motion for the gauge fields. The inclusive quark spectrum is discussed as well. We conclude the lecture with a discussion of the inclusive gluon spectrum at next-to-leading order and outline a proof of high energy factorization in this context. Understanding this factorization may hold the key to understanding early thermalization in heavy ion collisions. Some recent progress in this direction is briefly discussed.

2. Parton model, gluon saturation

In this lecture, we will begin with the simple parton model, and then discuss the physics of gluon saturation, which becomes crucial at small x.

2.1. DIS and the birth of the parton model

The parton model appeared to explain experimental results on Deep Inelastic Scattering (DIS). The basic idea of Deep Inelastic Scattering (DIS) is to use a well understood lepton probe (that does not involve strong interactions) to study a hadron. The interaction is via the exchange of a virtual photon[5]. Variants of this reaction involve the exchange of a $W^\pm$ or Z^0 boson which become increasingly important at large momentum transfers. The kinematics of DIS is characterized by a few Lorentz invariants (see figure 2 for the notations), traditionally defined as

$$\begin{aligned}\nu &\equiv P\cdot q\,,\\ s &\equiv (P+k)^2\,,\\ M_X^2 &\equiv (P+q)^2 = m_N^2+2\nu+q^2\,,\end{aligned}\tag{3}$$

where m_N is the nucleon mass (assuming that the target is a proton) and M_X the invariant mass of the hadronic final state. Because the exchanged photon

[5] If the virtuality of the photon is small (in *photo-production* reactions for instance), the assertion that the photon is a “well known probe that does not involve strong interactions” is not valid anymore. Indeed, the photon may fluctuate, for instance, into a ρ meson.

is space-like, one usually introduces $Q^2 \equiv -q^2 > 0$, and also $x \equiv Q^2/2\nu$. Note that since $M_X^2 \geq m_N^2$, we must have $0 \leq x \leq 1$ – the value $x = 1$ being reached only in the case where the proton is scattered elastically.

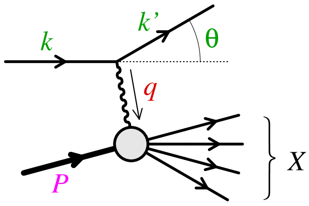

Fig. 2. Kinematical variables in the Deep Inelastic Scattering process. k and P are known from the experimental setup, and k' is obtained by measuring the deflected lepton.

The simplest cross-section one can measure in a DIS experiment is the total inclusive electron+proton cross-section, where one sums over all possible hadronic final states:

$$E'\frac{d\Sigma_{e^-N}}{d^3\boldsymbol{k}'} = \sum_{\text{states } X} E'\frac{d\Sigma_{e^-N\to e^-X}}{d^3\boldsymbol{k}'} \,. \tag{4}$$

This inclusive DIS cross-section can be written as

$$E'\frac{d\Sigma_{e^-N}}{d^3\boldsymbol{k}'} = \frac{1}{32\pi^3(s-m_N^2)}\frac{e^2}{q^4}4\pi L^{\mu\nu}W_{\mu\nu} \,, \tag{5}$$

where the *leptonic tensor* (neglecting the electron mass) is

$$\begin{aligned} L^{\mu\nu} &\equiv \left\langle \overline{u}(\boldsymbol{k}')\gamma^\mu u(\boldsymbol{k})\overline{u}(\boldsymbol{k})\gamma^\nu u(\boldsymbol{k}')\right\rangle_{\text{spin}} \\ &= 2(k^\mu k'^\nu + k^\nu k'^\mu - g^{\mu\nu}\, k\cdot k') \,, \end{aligned} \tag{6}$$

and $W_{\mu\nu}$ – the *hadronic tensor* — is defined as

$$4\pi W_{\mu\nu} \equiv \int d^4y\, e^{iq\cdot y} \left\langle \left\langle N(P)\middle| J_\nu^\dagger(y) J_\mu(0) \middle| N(P)\right\rangle\right\rangle_{\text{spin}} \,. \tag{7}$$

An important point is that $W_{\mu\nu}$ cannot be calculated by perturbative methods. This rank-2 tensor can be expressed simply in terms of two independent *structure functions*:

$$W_{\mu\nu} = -F_1\left(g_{\mu\nu} - \frac{q_\mu q_\nu}{q^2}\right) + \frac{F_2}{P\cdot q}\left(P_\mu - q_\mu\frac{P\cdot q}{q^2}\right)\left(P_\nu - q_\nu\frac{P\cdot q}{q^2}\right) \,. \tag{8}$$

As scalars, $F_{1,2}$ only depend on Lorentz invariants, namely, the variables x and Q^2. The inclusive DIS cross-section in the rest frame of the proton can be expressed in terms of $F_{1,2}$ as

$$\frac{d\Sigma_{e^-N}}{dE'd\Omega} = \frac{\alpha_{\rm em}^2}{4m_{_N} E^2 \sin^4(\theta/2)} \left[2\,F_1\,\sin^2\frac{\theta}{2} + \frac{m_{_N}^2}{\nu}\,F_2\,\cos^2\frac{\theta}{2}\right], \tag{9}$$

where Ω represents the solid angle of the scattered electron and E' its energy.

Two major experimental results from SLAC [7] in the late 1960's played a crucial role in the development of the parton model. The left plot of figure 3 shows the measured values of $F_2(x,Q^2)$ as a function of x. Even though the data covers a significant range in Q^2, all the data points seem to line up on a single curve, indicating that F_2 depends very little on Q^2 in this regime. This property is now known as *Bjorken scaling* [8]. In the right plot of figure 3, one sees a comparison of F_2 with the combination[6] $F_{_L} \equiv F_2 - 2x\,F_1$. Although there are few data points for $F_{_L}$, one can see that it is significantly lower than F_2 and close to zero[7]. As we shall see shortly, these two experimental facts already tell us a lot about the internal structure of the proton.

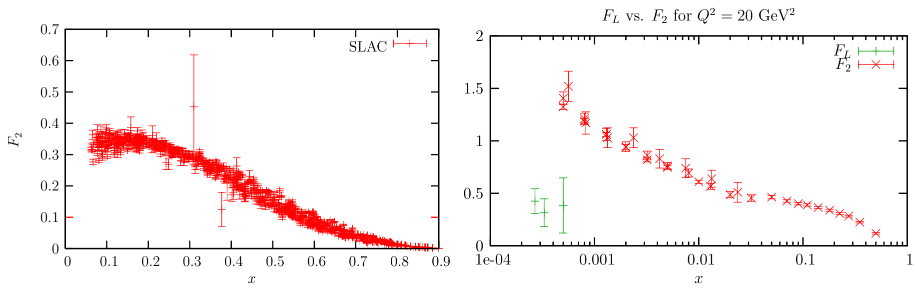

Fig. 3. SLAC results on DIS.

2.2. *Parton model at small x*

Let us now compute the hadronic tensor $W^{\mu\nu}$ for the DIS reaction on a point-like free fermion i carrying the fraction $x_{_F}$ of the proton momentum. Because we ignore interactions for the time being, this calculation (in

[6] $F_{_L}$, the longitudinal structure function, describes the inclusive cross-section between the proton and a longitudinally polarized proton.

[7] From current algebra, it was predicted that $F_2 = 2xF_1$; this relation is known as the *Callan–Gross relation* [9].

contrast to that for a proton target) can be done in closed form. We obtain,

$$4\pi W_i^{\mu\nu} = 2\pi x_{\rm F}\,\delta(x-x_{\rm F})\,e_i^2\left[-\left(g^{\mu\nu}-\frac{q^\mu q^\nu}{q^2}\right)\right.$$
$$\left.+\frac{2x_{\rm F}}{P\cdot q}\left(P^\mu-q^\mu\frac{P\cdot q}{q^2}\right)\left(P^\nu-q^\nu\frac{P\cdot q}{q^2}\right)\right], \qquad (10)$$

where e_i is the electric charge of the parton under consideration. Let us now assume that in a proton there are $f_i(x_{\rm F})dx_{\rm F}$ partons of type i with a momentum fraction between $x_{\rm F}$ and $x_{\rm F}+dx_{\rm F}$, and that the photon scatters incoherently off each of them. We would thus have

$$W^{\mu\nu} = \sum_i \int_0^1 \frac{dx_{\rm F}}{x_{\rm F}}\, f_i(x_{\rm F})\, W_i^{\mu\nu}\,. \qquad (11)$$

(The factor $x_{\rm F}$ in the denominator is a "flux factor".) At this point, we can simply read the values of $F_{1,2}$,

$$F_1 = \frac{1}{2}\sum_i e_i^2 f_i(x)\,, \quad F_2 = 2\,xF_1\,. \qquad (12)$$

We thus see that the two experimental observations of *(i)* Bjorken scaling and *(ii)* the Callan–Gross relation are automatically realized in this naive picture of the proton[8].

In the 1970's, after the advent of Quantum Chromodynamics and the discovery of asymptotic freedom by Gross, Politzer and Wilczek in 1973 [1], a more rigorous theoretical basis of the parton model has been developed. In particular, the Operator Product Expansion applied to the DIS reaction indicates that there are some violations to Bjorken scaling, and that these violations can be calculated using QCD perturbation theory via the DGLAP equation [5]. This machinery has now been pushed to higher orders (NNLO), leading to a very solid quantitative agreement between QCD predictions and measurements in DIS experiments, as illustrated in figure 4 (see for instance [13] for more details).

[8] In particular, $F_{\rm L}=0$ in this model is intimately related to the spin 1/2 structure of the scattered partons. Scalar partons, for instance, would give $F_1=0$, at variance with experimental results.

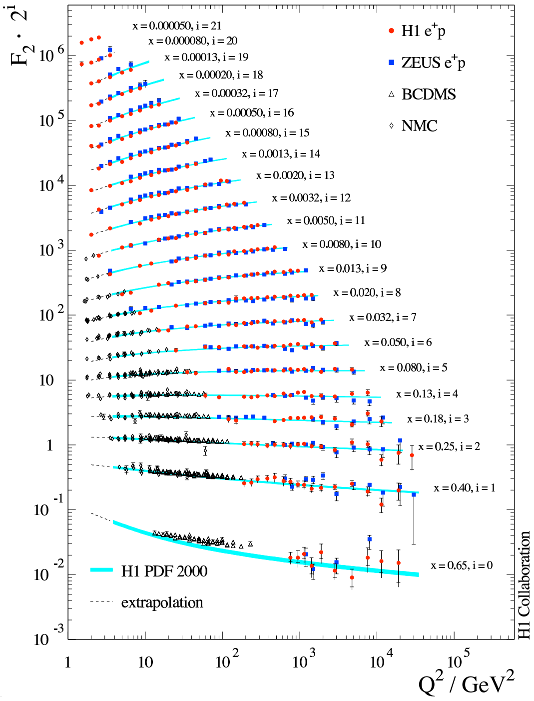

Fig. 4. Comparison of the measured F_2 with QCD fits.

2.3. Gluon evolution at small x

Before we proceed further, let us describe in qualitative terms (see [10] for instance) what a proton constituted of fermionic constituents bound by interactions involving the exchange of gauge bosons may look like. In the left panel of figure 5 are represented the three valence partons (quarks) of the proton. These quarks interact by gluon exchanges, and can also fluctuate into states that contain additional gluons (and also quark–antiquark pairs). These fluctuations can exist at any space-time scale smaller than the proton size (~ 1 fermi). (In this picture, one should think of the horizontal axis as

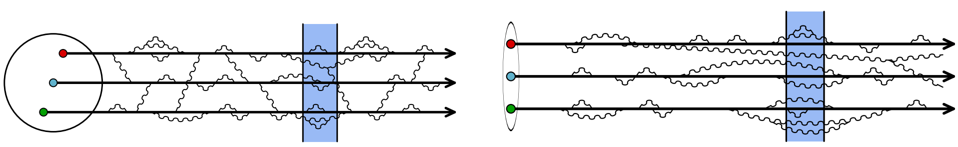

Fig. 5. Cartoons of the valence partons of a proton, and their interactions and fluctuations. Left: proton at low energy. Right: proton at high energy.

the time axis.) When one probes the proton in a scattering experiment, the probe (*e.g.* the virtual photon in DIS) is characterized by certain resolutions in time and in transverse coordinate. The shaded area in the picture is meant to represent the time resolution of the probe: any fluctuation which is shorter lived than this resolution cannot be seen by the probe, because it appears and dies out too quickly.

In the right panel of figure 5, the same proton is represented after a boost, while the probe has not changed. The main difference is that all the internal time scales are Lorentz dilated. As a consequence, the interactions among the quarks now take place over times much larger than the resolution of the probe. The probe therefore sees only free constituents. Moreover, this time dilation allows more fluctuations to be resolved by the probe; thus, a high energy proton appears to contain more gluons than a proton at low energy[9].

In fact, this growth of the gluon distribution at small x is observed experimentally,

$$xG(x,Q^2) \sim \frac{1}{x^\omega}\,. \tag{13}$$

However, the gluon distribution cannot grow at this pace indefinitely. Indeed, at some point, the occupation number of the gluons will become large and the recombination[10] of two gluons will become important. This phenomenon is known as *gluon saturation* [20]. In the linear regime, described by the BFKL equation, each valence parton from the proton initiates its own gluon ladder that evolves independently from the others. In the saturated regime, these gluon ladders can merge, thereby reducing the growth of the gluon distribution. The effect of these recombinations on the scattering amplitude is taken into account by the non-linear term of the BK equation.

A semi quantitative criterion for gluon saturation can be obtained [20] by comparing the surface density of gluons, $\rho \sim xG(x,Q^2)/\pi R^2$, and the cross-section for gluon recombination, $\Sigma \sim \alpha_s/Q^2$. Saturation occurs when $1 \lesssim \rho\Sigma$, *i.e.* when

$$Q^2 \le Q_s^2\,, \quad \text{with} \quad Q_s^2 \sim \frac{\alpha_s xG(x,Q_s^2)}{\pi R_A^2} \sim A^{1/3}\frac{1}{x^{0.3}}\,. \tag{14}$$

The quantity Q_s is known as the *saturation momentum.* Its dependence on the number of nucleons A (in the case of a nuclear target) comes from the fact that $xG(x,Q^2)$ scales like the volume, while πR^2 is an area. Its x dependence is a phenomenological parameterization inspired by from fits

[9] Equivalently, if the energy of the proton is fixed, there are more gluons at lower values of the momentum fraction x_F.

[10] The DGLAP evolution equation, as well as the BFKL equation, includes only gluon splittings.

of HERA data. From Eq. (14), one can divide the x, Q^2 in two regions, as illustrated in figure 6. The saturated regime corresponds to the domain of low Q and low x.

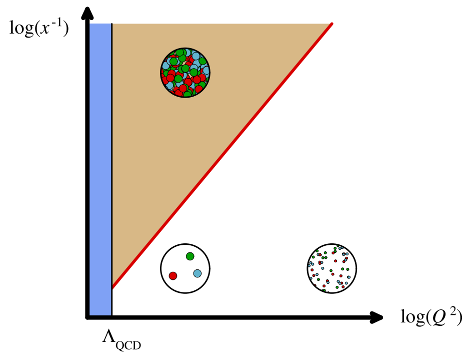

Fig. 6. Saturation domain in the x, Q^2 plane.

An effective description of the wavefunction of a hadron in the saturation regime, known as the *Color Glass Condensate*, has been developed. In the CGC description, one divides the degrees of freedom in the proton into fast partons (large x) and slow partons (small x) [21]. The fast partons are affected by time dilation, and do not have any significant time evolution during the brief duration of the collision; therefore, they are treated as static objects that carry a color source. These color sources produce a current, $J^\mu = \delta^{\mu +}\delta(x^-)\rho(\boldsymbol{x}_\perp)$, written here for a projectile moving in the $+z$ direction. The function $\rho(\boldsymbol{x}_\perp)$ describes the distribution of color charge as a function of the impact parameter. The slow partons, on the other hand, have a non trivial dynamics during the collision, and must be treated as gauge fields. The only coupling between the fast and slow partons is a coupling $A_\mu J^\mu$ between the color current of the fast partons and the gauge fields, which allows the fast partons to radiate slower partons by bremsstrahlung.

Because the configuration of the fast partons prior to the collision is different in every collision, the function $\rho(\boldsymbol{x}_\perp)$ must be a stochastic quantity, for which one can only specify a distribution $W_Y[\rho]$. Observables like cross-sections must be averaged over all the possible configurations of ρ with this distribution,

$$\big\langle \cdots \big\rangle \equiv \int \big[D\rho\big]\, W_Y[\rho] \, \cdots \,. \tag{15}$$

A crucial point is that the distribution $W_Y[\rho]$ depends on Y, the rapidity that separates what is considered fast and slow. Because such a separation is arbitrary, physical quantities cannot depend on it; one can derive from this requirement a renormalization group equation for $W_Y[\rho]$ — known as the *JIMWLK equation* [22] — of the form:

$$\frac{\partial W_{_Y}[\rho]}{\partial Y} = \mathcal{H}[\rho]\, W_{_Y}[\rho]\,. \tag{16}$$

The *JIMWLK Hamiltonian* $\mathcal{H}[\rho]$ contains first and second derivatives with respect to the source ρ,

$$\mathcal{H}[\rho] = \int\limits_{\boldsymbol{x}_\perp} \varSigma(\boldsymbol{x}_\perp)\frac{\delta}{\delta\rho(\boldsymbol{x}_\perp)} + \frac{1}{2}\int\limits_{\boldsymbol{x}_\perp,\boldsymbol{y}_\perp} \chi(\boldsymbol{x}_\perp,\boldsymbol{y}_\perp)\frac{\delta^2}{\delta\rho(\boldsymbol{x}_\perp)\delta\rho(\boldsymbol{y}_\perp)}\,, \tag{17}$$

where $\varSigma(\boldsymbol{x}_\perp)$ and $\chi(\boldsymbol{x}_\perp,\boldsymbol{y}_\perp)$ are known functionals of ρ.

In lecture II, we will derive an equivalent form of this evolution equation, known as the Balitsky's equations, that applies directly to scattering amplitudes — in particular to the dipole scattering amplitude,

$$\langle \boldsymbol{T}(\boldsymbol{x}_\perp,\boldsymbol{y}_\perp)\rangle = \int [D\rho]\; W_{_Y}[\rho]\,\left[1-\frac{1}{N_c}\mathrm{tr}(U(\boldsymbol{x}_\perp)U^\dagger(\boldsymbol{y}_\perp))\right]\,, \tag{18}$$

where the Wilson line U is evaluated in the color field generated by the configuration ρ of the color sources.

Eq. (16) predicts the energy dependence of the distribution of sources. However, it must be supplemented by an initial condition at some Y_0. As with the DGLAP equation, the initial condition is non-perturbative, and one must in general model it or guess it from experimental data. In the case of large nuclei, one often uses the *McLerran–Venugopalan model*, which assumes that $W_{_{Y_0}}[\rho]$ is a Gaussian [21, 23, 24]:

$$W_{_{Y_0}}[\rho] = \exp\left[-\int d^2\boldsymbol{x}_\perp \frac{\rho(\boldsymbol{x}_\perp)\rho(\boldsymbol{x}_\perp)}{2\mu^2(\boldsymbol{x}_\perp)}\right]\,. \tag{19}$$

The idea behind this model is that the color charge per unit area, $\rho(\boldsymbol{x}_\perp)$, is the sum of the color charges of the partons that sit at approximately the same impact parameter. In a large nucleus, this will be the sum of a large number of random charges; for $N_c = 3$, this leads to a Gaussian distribution for ρ plus a small (albeit physically very relevant) contribution from the cubic Casimir [24]. The fact that this Gaussian has only correlations local in impact parameter is a consequence of confinement: color charges separated by more than the nucleon size cannot be correlated. The MV model is generally used at a moderately small x, of the order of 10^{-2}. If the problem under consideration requires smaller values of x, one should use the BK or JIMWLK equations, with the MV distribution as the initial condition.

3. Saturation in DIS

In the first lecture, we have introduced the parton model and we have presented a qualitative introduction to gluon saturation. In this lecture, we study more specifically saturation effects in DIS. In particular, we derive the energy dependence of these processes, by deriving the Balitsky–Kovchegov equation. We also show how saturation provides a natural explanation for the observed "geometrical scaling".

3.1. Eikonal scattering

Before going to the main subject of this lecture, let us recall an important result concerning the high energy limit of the scattering amplitude of some state off an external field [14]. Consider the generic S-matrix element

$$S_{\beta\alpha} \equiv \big\langle \beta_{\rm out} \big| \alpha_{\rm in} \big\rangle = \big\langle \beta_{\rm in} \big| U(+\infty, -\infty) \big| \alpha_{\rm in} \big\rangle \,, \tag{20}$$

for the transition from a state α to a state β, where

$$U(+\infty, -\infty) = T_+ \, \exp\left[i \int d^4x \, \mathcal{L}_{\rm int}(\phi_{\rm in}(x)) \right] \tag{21}$$

is the evolution operator from $t = -\infty$ to $t = +\infty$. (T_+ denotes an ordering in the light-cone time x^+.) The interaction Lagrangian $\mathcal{L}_{\rm int}$ contains both the self-interactions of the fields and their interactions with the external field. Now apply a boost in the z direction to all the particles contained in the states α and β. Formally, this can be done by multiplying the states by $\exp(-i\omega K^3)$, where ω is the rapidity of the boost and K^3 the generator of longitudinal boosts. Our goal is to compute the limit $\omega \to +\infty$ of the transition amplitude,

$$S^{(\infty)}_{\beta\alpha} \equiv \lim_{\omega\to+\infty} \big\langle \beta_{\rm in} \big| e^{i\omega K^3} U(+\infty, -\infty) e^{-i\omega K^3} \big| \alpha_{\rm in} \big\rangle \,. \tag{22}$$

The behavior of scattering amplitudes in this limit is easy to understand. The time spent by the incoming particles in the region where the external field is acting goes to zero as the inverse of the collision energy E. If the coupling to the external field was purely scalar, this would imply that the scattering amplitude itself goes to zero as E^{-1}. However, in the case of a vector coupling, the longitudinal component of the current increases as E, which compensates the decrease in the interaction time, thereby leading to a finite (non-zero and non infinite) high energy limit. For this reason, let us assume that the coupling of the fields to the external potential is of the form $g\,\mathcal{A}_\mu(x) J^\mu(x)$ where J^μ is a vector current built from the elementary fields of the theory under consideration.

The high energy limit of the transition amplitude reads

$$S^{(\infty)}_{\beta\alpha} = \sum_\delta \int \left[\prod_{i\in\delta} \frac{dk_i^+}{4\pi k_i^+} d^2\boldsymbol{x}_{i\perp}\right] \Psi^\dagger_{\delta\beta}(\{k_i^+, \boldsymbol{x}_{i\perp}\}) \left[\prod_{i\in\delta} U_i(\boldsymbol{x}_{i\perp})\right] \Psi_{\delta\alpha}(\{k_i^+, \boldsymbol{x}_{i\perp}\})\,, \tag{23}$$

where the $\Psi_{\delta\alpha}$ and $\Psi_{\delta\beta}$ are the light-cone wavefunctions of the initial and final state, for the Fock component where the intermediate state is δ. The factors $U_i(\boldsymbol{x}_\perp)$ are known as *Wilson lines*:

$$U_i(\boldsymbol{x}_\perp) \equiv T_+ \exp\left[ig_{_i} \int dx^+\, \mathcal{A}^-_a(x^+, 0, \boldsymbol{x}_\perp) t^a\right]. \tag{24}$$

Wilson lines resum multiple scatterings off the external field, as one can see by expanding the exponential. Thus, the physical picture of high energy scattering off some external field is that the initial state evolves from $-\infty$ to 0, multiply scatters during an infinitesimally short time off the external potential, and evolves again from 0 to $+\infty$ to form the final state.

3.2. BFKL equation

Let us now derive the BFKL equation. Our derivation is inspired from [15–19]. Consider the forward scattering off an external field of a state α whose simplest Fock component is a color singlet quark–antiquark pair. Thus, the transition amplitude can be written as

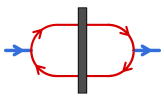

$$= \left|\Psi^{(0)}(\boldsymbol{x}_\perp, \boldsymbol{y}_\perp)\right|^2 \mathrm{tr}\left[U(\boldsymbol{x}_\perp) U^\dagger(\boldsymbol{y}_\perp)\right]. \tag{25}$$

We will not need to specify more the light-cone wavefunction of the state under consideration. Note that the product of the two Wilson lines is traced, because the state α is color singlet. A crucial property of this transition amplitude is that it is completely independent of the collision energy. However, as we shall see, a non trivial energy dependence arises in this amplitude because of large logarithms in loop corrections.

Consider now the 1-loop corrections to this amplitude depicted in figure 7. These 1-loop corrections all involve one additional gluon attached to the quark or antiquark lines. In some of the corrections, that we shall call *real corrections*, the gluon is present in the state that goes through the external field. In the other corrections, the *virtual corrections*, the gluon is just a fluctuation in the wavefunction of the initial or final state. The calculation of these diagrams is straightforward in the impact parameter representation.

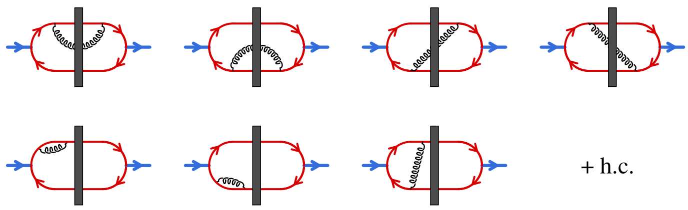

Fig. 7. One-loop corrections to the scattering of a dipole off an external field. Only half of the virtual corrections have been represented.

One simply needs the formula for the $q\bar{q}g$ vertex:

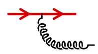

$$= 2gt^a\,\frac{\boldsymbol{\epsilon}_\lambda\cdot\boldsymbol{k}_\perp}{k_\perp^2} = \int d^2\boldsymbol{r}_\perp\, e^{-i\boldsymbol{k}_\perp\cdot\boldsymbol{r}_\perp}\,\frac{2ig}{2\pi}t^a\frac{\boldsymbol{\epsilon}_\lambda\cdot\boldsymbol{r}_\perp}{r_\perp^2}\,, \tag{26}$$

where $\boldsymbol{\epsilon}_\lambda$ is the polarization vector of the gluon and $\boldsymbol{k}_\perp$ its transverse momentum. Armed with these tools, it is easy to obtain expressions such as

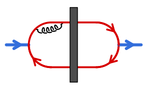

$$\begin{aligned} &= \left|\Psi^{(0)}(\boldsymbol{x}_\perp,\boldsymbol{y}_\perp)\right|^2 \mathrm{tr}\left[t^a t^a U(\boldsymbol{x}_\perp)U^\dagger(\boldsymbol{y}_\perp)\right] \\ &\quad\times -2\alpha_{\mathrm{s}}\int\frac{dk^+}{k^+}\int\frac{d^2\boldsymbol{z}_\perp}{(2\pi)^2}\frac{(\boldsymbol{x}_\perp-\boldsymbol{z}_\perp)\cdot(\boldsymbol{x}_\perp-\boldsymbol{z}_\perp)}{(\boldsymbol{x}_\perp-\boldsymbol{z}_\perp)^2(\boldsymbol{x}_\perp-\boldsymbol{z}_\perp)^2}\,. \end{aligned} \tag{27}$$

We find that the sum of all the virtual corrections reads

$$\begin{aligned} &-\frac{C_{\mathrm{f}}\alpha_{\mathrm{s}}}{\pi^2}\int\frac{dk^+}{k^+}\int d^2\boldsymbol{z}_\perp\,\frac{(\boldsymbol{x}_\perp-\boldsymbol{y}_\perp)^2}{(\boldsymbol{x}_\perp-\boldsymbol{z}_\perp)^2(\boldsymbol{y}_\perp-\boldsymbol{z}_\perp)^2} \\ &\times\left|\Psi^{(0)}(\boldsymbol{x}_\perp,\boldsymbol{y}_\perp)\right|^2\mathrm{tr}\left[U(\boldsymbol{x}_\perp)U^\dagger(\boldsymbol{y}_\perp)\right]\,, \end{aligned} \tag{28}$$

where $C_{\mathrm{f}} \equiv t^a t^a = (N^2-1)/2N$ for SU(N). In this formula, k^+ is the longitudinal momentum of the gluon. As one can see, there is a logarithmic divergence in the integration over this variable. The lower bound should arguably be some non-perturbative hadronic scale Λ, and the upper bound must be the longitudinal momentum p^+ of the quark or antiquark that emitted the photon. Hence we have a $\log(p^+/\Lambda)$, which is a large factor in the limit of high-energy (strictly speaking, the high-energy limit is ill defined because of these corrections). The calculation of the real corrections is a bit more involved. For instance, one has

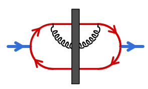

$$\begin{aligned} &= \left|\Psi^{(0)}(\boldsymbol{x}_\perp,\boldsymbol{y}_\perp)\right|^2\mathrm{tr}\left[t^a U(\boldsymbol{x}_\perp)t^b U^\dagger(\boldsymbol{y}_\perp)\right] \\ &\times\ 4\alpha_{\mathrm{s}}\int\frac{dk^+}{k^+}\int\frac{d^2\boldsymbol{z}_\perp}{(2\pi)^2}\widetilde{U}_{ab}(\boldsymbol{z}_\perp)\frac{(\boldsymbol{x}_\perp-\boldsymbol{z}_\perp)\cdot(\boldsymbol{x}_\perp-\boldsymbol{z}_\perp)}{(\boldsymbol{x}_\perp-\boldsymbol{z}_\perp)^2(\boldsymbol{x}_\perp-\boldsymbol{z}_\perp)^2}\,, \end{aligned} \tag{29}$$

where $\widetilde{U}_{ab}(\boldsymbol{z}_\perp)$ is a Wilson line in the adjoint representation that represents the eikonal phase factor associated to the gluon ($\boldsymbol{z}_\perp$ is the impact parameter of the gluon). In order to simplify the real terms, we need the following relation between fundamental and adjoint Wilson lines, $t^a\widetilde{U}_{ab}(\boldsymbol{z}_\perp) = U(\boldsymbol{z}_\perp)t^bU^\dagger(\boldsymbol{z}_\perp)$, and the Fierz identity obeyed by fundamental SU(N) matrices: $t^b_{ij}t^b_{kl} = \frac{1}{2}\delta_{il}\delta_{jk} - \frac{1}{2N}\delta_{ij}\delta kl$. Thanks to these identities, one can rewrite all the real corrections in terms of the quantity $\boldsymbol{S}(\boldsymbol{x}_\perp,\boldsymbol{y}_\perp) \equiv \mathrm{tr}\left[U(\boldsymbol{x}_\perp)U^\dagger(\boldsymbol{y}_\perp)\right]/N$. Collecting all the terms, and summing real and virtual contributions, we obtain the following expression for the 1-loop transition amplitude

$$-\frac{\alpha_\mathrm{s}N^2Y}{2\pi^2}\left|\Psi^{(0)}(\boldsymbol{x}_\perp,\boldsymbol{y}_\perp)\right|^2\int d^2\boldsymbol{z}_\perp\,\frac{(\boldsymbol{x}_\perp-\boldsymbol{y}_\perp)^2}{(\boldsymbol{x}_\perp-\boldsymbol{z}_\perp)^2(\boldsymbol{y}_\perp-\boldsymbol{z}_\perp)^2}$$
$$\times\Big\{\boldsymbol{S}(\boldsymbol{x}_\perp,\boldsymbol{y}_\perp)-\boldsymbol{S}(\boldsymbol{x}_\perp,\boldsymbol{z}_\perp)\boldsymbol{S}(\boldsymbol{z}_\perp,\boldsymbol{y}_\perp)\Big\}, \tag{30}$$

where we denote $Y \equiv \ln(p^+/\Lambda)$. This correction to the transition amplitude is not small when $\alpha_\mathrm{s}^{-1} \lesssim Y$, which means that n-loop contributions should be considered in order to resum all the powers $(\alpha_\mathrm{s}Y)^n$. Here, we are just going to admit that this n-loop calculation amounts to exponentiating the 1-loop result. In other words, Eq. (30) is sufficient in order to obtain the derivative $\partial\boldsymbol{S}/\partial Y$,

$$\frac{\partial\boldsymbol{S}(\boldsymbol{x}_\perp,\boldsymbol{y}_\perp)}{\partial Y} = -\frac{\alpha_\mathrm{s}N_c}{2\pi^2}\int d^2\boldsymbol{z}_\perp\,\frac{(\boldsymbol{x}_\perp-\boldsymbol{y}_\perp)^2}{(\boldsymbol{x}_\perp-\boldsymbol{z}_\perp)^2(\boldsymbol{y}_\perp-\boldsymbol{z}_\perp)^2}$$
$$\times\Big\{\boldsymbol{S}(\boldsymbol{x}_\perp,\boldsymbol{y}_\perp)-\boldsymbol{S}(\boldsymbol{x}_\perp,\boldsymbol{z}_\perp)\boldsymbol{S}(\boldsymbol{z}_\perp,\boldsymbol{y}_\perp)\Big\}. \tag{31}$$

It is customary to rewrite this equation in terms of T-matrix elements, $\boldsymbol{T}(\boldsymbol{x}_\perp,\boldsymbol{y}_\perp) \equiv 1-\boldsymbol{S}(\boldsymbol{x}_\perp,\boldsymbol{y}_\perp)$. The BFKL equation [4] describes the regime where $\boldsymbol{T}(\boldsymbol{x}_\perp,\boldsymbol{y}_\perp)$ is small, so that we can neglect the terms that are quadratic in $\boldsymbol{T}$. It reads:

$$\frac{\partial\boldsymbol{T}(\boldsymbol{x}_\perp,\boldsymbol{y}_\perp)}{\partial Y} = \frac{\alpha_\mathrm{s}N_c}{2\pi^2}\int d^2\boldsymbol{z}_\perp\,\frac{(\boldsymbol{x}_\perp-\boldsymbol{y}_\perp)^2}{(\boldsymbol{x}_\perp-\boldsymbol{z}_\perp)^2(\boldsymbol{y}_\perp-\boldsymbol{z}_\perp)^2}$$
$$\times\Big\{\boldsymbol{T}(\boldsymbol{x}_\perp,\boldsymbol{z}_\perp)+\boldsymbol{T}(\boldsymbol{z}_\perp,\boldsymbol{y}_\perp)-\boldsymbol{T}(\boldsymbol{x}_\perp,\boldsymbol{y}_\perp)\Big\}. \tag{32}$$

One can verify easily that $\boldsymbol{T}=0$ is a *fixed point* of this equation (the right hand side vanishes if one sets $\boldsymbol{T}=0$), but that this fixed point is unstable (if one sets $\boldsymbol{T}=\epsilon>0$, the right hand side is positive). Since there are no other fixed points, solutions of the BFKL have an unbounded growth in the high energy limit ($Y\to+\infty$). This behavior, however, is not physical because the unitarity of scattering amplitude implies that $\boldsymbol{T}(\boldsymbol{x}_\perp,y_\perp)$ should not become greater than unity.

3.3. Balitsky–Kovchegov equation

The solution to the above problem was in fact already contained in Eq. (31). When written in terms of $\boldsymbol{T}$ without assuming that $\boldsymbol{T}$ is small,

$$\frac{\partial\,\boldsymbol{T}(\boldsymbol{x}_\perp,\boldsymbol{y}_\perp)}{\partial Y} = \frac{\alpha_{\rm s} N_c}{2\pi^2}\int d^2\boldsymbol{z}_\perp\,\frac{(\boldsymbol{x}_\perp-\boldsymbol{y}_\perp)^2}{(\boldsymbol{x}_\perp-\boldsymbol{z}_\perp)^2(\boldsymbol{y}_\perp-\boldsymbol{z}_\perp)^2}$$
$$\times\Big\{\boldsymbol{T}(\boldsymbol{x}_\perp,\boldsymbol{z}_\perp)+\boldsymbol{T}(\boldsymbol{z}_\perp,\boldsymbol{y}_\perp)-\boldsymbol{T}(\boldsymbol{x}_\perp,\boldsymbol{y}_\perp)-\boldsymbol{T}(\boldsymbol{x}_\perp,\boldsymbol{z}_\perp)\boldsymbol{T}(\boldsymbol{z}_\perp,\boldsymbol{y}_\perp)\Big\}\,, \quad (33)$$

it has a non-linear term that confines $\boldsymbol{T}$ to the range $[0,1]$. Indeed, the presence of this quadratic term makes $\boldsymbol{T}=1$ a stable fixed point of the equation. Therefore, the generic behavior of solutions of Eq. (33) is that $\boldsymbol{T}$ starts at small values at small Y and asymptotically reaches the value $\boldsymbol{T}=1$ in the high energy limit. Eq. (33) is known as the *Balitsky–Kovchegov equation* [17, 18].

The interaction of a color singlet dipole with an external color field is a possible description of DIS, in a frame in which the virtual photon splits into a quark–antiquark pair long before it collides with the proton (the external color field would represent the proton target). Although it is legitimate to treat the proton as a frozen configuration of color field due to the brevity of the interaction, we do not know what this field is. Moreover, since this field is created by the partons inside the proton, that have a complicated dynamics, this color field must be different for each collision, and should therefore be treated as random. Therefore, in order to turn our dipole scattering amplitude into an object that we could use to compute the DIS cross-section at high-energy, we must average over all the possible configurations of the external field. Let us denote by $\big\langle\cdots\big\rangle$ this average. The effect of this average on the energy dependence of the amplitude is simply taken into account by taking the average of Eq. (33). However, one sees that the evolution equation for $\big\langle\boldsymbol{T}\big\rangle$ involves in its right hand side the average of a product of two $\boldsymbol{T}$'s, $\big\langle\boldsymbol{T}\boldsymbol{T}\big\rangle$. Therefore, we do not have a closed equation anymore. An evolution equation for $\big\langle\boldsymbol{T}\boldsymbol{T}\big\rangle$ could be obtained by the same procedure, which would depend on yet another new object, and so on. At the end of the day, one in fact obtains an infinite hierarchy of nested equations, known as *Balitsky's equations* [18]. This hierarchy of evolution equations is equivalent to the JIMWLK equation — presented in the previous lecture.

It is only if one assumes that the averages of products of amplitudes factorize into products of averages, $\langle\boldsymbol{T}\,\boldsymbol{T}\rangle\approx\langle\boldsymbol{T}\rangle\,\langle\boldsymbol{T}\rangle$, that this hierarchy can be truncated into a closed equation which is identical to Eq. (33) — the BK equation — with $\boldsymbol{T}$ replaced by $\big\langle\boldsymbol{T}\big\rangle$. This approximation amounts to drop certain correlations among the target fields, and is believed to be a good approximation for a large nucleus in the limit of a large number of colors [17].

3.4. Analogies with reaction–diffusion processes

There are interesting analogies between the evolution equations that govern the energy dependence of scattering amplitude in QCD and simple models of *reaction–diffusion processes* [25]. The simplest setting in which these correspondences can be seen is to consider the dipole scattering amplitude off a large nucleus, and to assume translation and rotation invariance in impact parameter space. It is useful to define its Fourier transform as

$$N(Y,k_\perp) \equiv 2\pi \int d^2\boldsymbol{x}_\perp\, e^{i\boldsymbol{k}_\perp\cdot\boldsymbol{x}_\perp}\,\frac{\left<\boldsymbol{T}(0,\boldsymbol{x}_\perp)\right>_Y}{x_\perp^2}\,. \tag{34}$$

(Note the factor $1/x_\perp^2$ included in this definition.) It turns out that for this object N, the BK equation has a very simple non-linear term,

$$\frac{\partial N(Y,k_\perp)}{\partial Y} = \frac{\alpha_{\rm s}N_c}{\pi}\Big[\chi(-\partial_L)N(Y,k_\perp) - N^2(Y,k_\perp)\Big]\,. \tag{35}$$

In this equation, $L \equiv \ln(k_\perp^2/k_0^2)$ and $\chi(\gamma) \equiv 2\psi(1) - \psi(\gamma) - \psi(1-\gamma)$ with $\psi(\boldsymbol{z}) \equiv d\ln\Gamma(z)/dz$. The function $\chi(\gamma)$ has poles at $\gamma = 0$ and $\gamma = 1$, and a minimum at $\gamma = 1/2$. By expanding it up to quadratic order around its minimum, and by defining new variables,

$$t \sim Y\,,\quad z \sim L + \frac{\alpha_{\rm s}N_c}{2\pi}\chi''\left(\frac{1}{2}\right)Y\,, \tag{36}$$

the BK equation simplifies into

$$\partial_t N = \partial_z^2 N + N - N^2\,, \tag{37}$$

known as the *Fisher–Kolmogorov–Petrov–Piscounov (FKPP) equation*. This equation has been extensively studied in the literature, because it is the simplest realization of the so-called reaction–diffusion processes. It describes the evolution of a number N of objects that live in one spatial dimension. The diffusion term $\partial_z^2 N$ describes the fact that these entities can hop from one location to neighboring locations. The positive linear term $+N$ means that an object can split into two, and the negative quadratic term $-N^2$ that two objects can merge into a single one. One can easily check that this equation has two fixed points, $N = 0$ which is unstable and $N = 1$ which is stable.

An important property of this equation is that it admits *asymptotic traveling waves* as solutions. Let us assume that the initial condition $N(t_0, z)$ goes to 1 at $z \to -\infty$ and to 0 at $z \to +\infty$, with an exponential tail

$N(t_0,z) \underset{z\to+\infty}{\sim} \exp(-\beta z)$. If the slope of the exponential obeys $\beta > 1$, the solution at late time depends only on a single variable,

$$N(t,z) \underset{t\to+\infty}{\sim} N\left(z - 2t - \frac{3}{2}\ln(t)\right) . \tag{38}$$

When $t \to +\infty$, the logarithm can be neglected in front of the term linear in time, and one has a traveling wave moving at a constant velocity $dz/dt = 2$ without deformation. Moreover, this velocity is independent of the details of the initial condition for a large class of initial conditions.

Going back to the dipole scattering amplitude, this result implies the following scaling behavior at large Y:

$$\left\langle \boldsymbol{T}(0,\boldsymbol{x}_\perp)\right\rangle_Y = T(Q_{\rm s}(Y)x_\perp) , \tag{39}$$

with a saturation scale of the form $Q_{\rm s}^2(Y) = k_0^2\, Y^{-\delta}\, e^{\omega Y}$. (The exponential comes from the constant in the velocity of the traveling wave, and the power law correction comes from the subleading logarithm.) This scaling property has an interesting phenomenological consequence for the inclusive DIS cross-section, that one can express in terms of the forward dipole scattering amplitude thanks to the optical theorem:

$$\varSigma_{\gamma^* p}(Y,Q^2) = \varSigma_0 \int d^2\boldsymbol{x}_\perp \int_0^1 dz\, \left|\psi(z,x_\perp,Q^2)\right|^2 \left\langle \boldsymbol{T}(0,\boldsymbol{x}_\perp)\right\rangle_Y . \tag{40}$$

In this formula, $\psi(z,x_\perp,Q^2)$ is the light-cone wave function for a photon of virtuality Q^2 that splits into a quark–antiquark dipole of size $\boldsymbol{x}_\perp$, the quark carrying the fraction z of the longitudinal momentum of the photon. This wavefunction can be calculated in QED, and its only property that we need here is that it depends only on the combination $[m^2+Q^2z^2(1-z)^2]\boldsymbol{x}_\perp^2$ where m is the quark mass. If one neglects the quark mass, then Eq. (39) implies a simple scaling for the $\gamma^* p$ cross-section itself: $\varSigma_{\gamma^* p}(Y,Q^2) = \varSigma_{\gamma^* p}(Q^2/Q_{\rm s}^2(Y))$. Such a *geometrical scaling* [26] has been found in the DIS experimental results[11], as shown in figure 8. A comment is in order here; as the approach based on collinear factorization and the DGLAP equation succeeds at reproducing much of the inclusive DIS data, it certainly also reproduces this scaling that is present in the data. However, this approach does not provide an explanation for the scaling. It arises via some fine tuning of the initial condition for the DGLAP evolution. In contrast, in the Color Glass Condensate description of DIS, this scaling is almost automatic.

[11] In addition to explaining geometrical scaling, saturation inspired fits of DIS data are quite successful at small x. See [27].

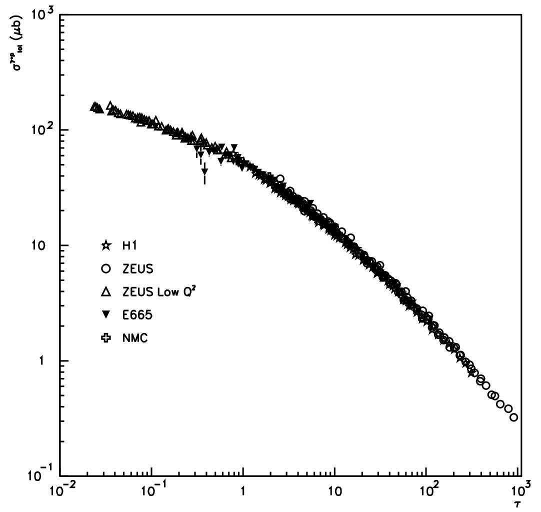

Fig. 8. Photon–proton total cross-section measured at HERA, displayed against $\tau \equiv Q^2/Q_s^2(Y)$.

4. Nucleus–nucleus collisions

4.1. Introduction

Up to now, we only considered DIS, in which a possibly saturated proton or nucleus is probed by an elementary object[12] — a virtual photon that has fluctuated into a quark–antiquark dipole. In such a situation, the scattering amplitude can be written in closed form as a product of Wilson lines, and its energy dependence can be obtained either from Balitsky's equations or from the JIMWLK evolution of the distribution of sources that produce the color field of the proton. There are, however, interesting problems that involve two densely occupied projectiles. The archetype of such a situation is a high-energy nucleus–nucleus collision. In these collisions, one of the main challenges is to calculate the multiplicity of the particles (gluons at leading order) that are produced at the impact of the two nuclei. In the Color Glass Condensate framework, one has to couple the gauge fields to a current that receives contributions from the color sources of the two projectiles,

$$J^\mu = \delta^{\mu +}\delta(x^-)\rho_1(\boldsymbol{x}_\perp) + \delta^{\mu -}\delta(x^+)\rho_2(\boldsymbol{x}_\perp)\,. \tag{41}$$

The fact that there are two strong sources leads to complications that are two-fold:

[12] Proton–nucleus collisions also belong to this category. Examples of processes have been studied in [28].

- there is no explicit formula that gives the multiplicity (or any other observable) in terms of Wilson lines in the collision of two saturated projectiles,
- if one is interested by the particle spectrum at some rapidity Y, one must evolve the two projectiles from their respective beam rapidity to Y. The question of the factorization of the large logarithms of $1/x$ is now much more complicated than in DIS.

The complications one is facing in this problem are illustrated in figure 9. In the saturated regime, reactions initiated by more than one parton (color source in the CGC description) in each projectile are important, and there can be a superposition of many independent scatterings, that will appear as disconnected graphs.

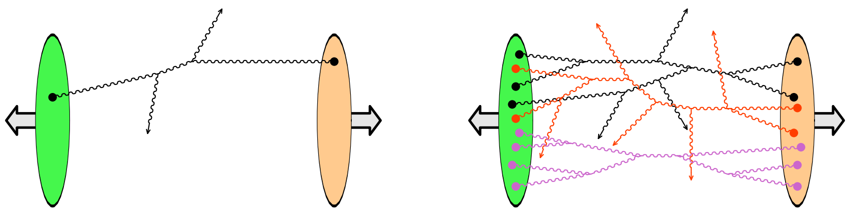

Fig. 9. Typical contributions to gluon production in hadronic collisions. The dots denote the color sources. Left: dilute regime. Right: saturated regime.

4.2. Power counting and bookkeeping

In the saturated regime, the color density ρ (represented by dots in figure 9) is non-perturbatively large $\rho \sim g^{-1}$. This is due to the fact that the occupation number, proportional to $\langle\rho\rho\rangle$, is of order α_s^{-1} in this regime. Thus for a *connected* graph, the order in g is given by

$$\frac{1}{g^2}\, g^{n_g}\, g^{2n_L}\,, \tag{42}$$

where n_g is the number of produced gluons and n_L the number of loops. One can see that this formula is independent of the number of sources ρ attached to the graph. Indeed, since each source brings a factor g^{-1} and is attached at a vertex that brings a factor g, each source counts as a factor 1. If the diagram under consideration is made of several disconnected subgraphs, one should apply Eq. (42) to each of them separately.

Among all the diagrams that appear in the calculation of particle production, a special role is played by the so-called *vacuum diagrams* — diagrams that have $n_g = 0$ external gluons. They only connect sources of the two projectiles, and are thus contributions to the vacuum-to-vacuum amplitude $\big\langle 0_{\rm out}\big|0_{\rm in}\big\rangle$, hence their name. The order of connected vacuum diagrams is $g^{2(n_{\rm L}-1)}$. An extremely useful property is that the sum of all the vacuum diagrams (connected or not) is the exponential of those that are connected (that we denote $iV[j]$ where j is the external current due to the color sources of the two projectiles)

$$\sum\begin{pmatrix}\text{all the vacuum}\\ \text{diagrams}\end{pmatrix} = \exp\left\{\sum\begin{pmatrix}\text{connected}\\ \text{vacuum diagrams}\end{pmatrix}\right\} \equiv e^{iV[j]}\,. \quad (43)$$

The reason why vacuum diagrams are important in our problem is that it is possible to write all the time ordered products of fields — that enter in the reduction formulas for gluon production amplitudes — as derivatives of $\exp(iV[j])$

$$\big\langle 0_{\rm out}\big|TA(x_1)\cdots A(x_n)\big|0_{\rm in}\big\rangle = \frac{\delta}{i\delta j(x_1)}\cdots\frac{\delta}{i\delta j(x_n)}\;e^{iV[j]}\,. \quad (44)$$

Thanks to this property, one can write a very compact formula for the probability P_n of producing exactly n gluons in the collision [29–31],

$$P_n = \frac{1}{n!}\,\mathcal{D}^n\,e^{iV[j_+]}\,e^{-iV^*[j_-]}\Big|_{j_+=j_-=j}\,, \quad (45)$$

where the operator $\mathcal{D}$ is defined by[13]

$$\begin{cases}\mathcal{D} \equiv \displaystyle\int\limits_{x,y} G^0_{+-}(x,y)\,\square_x\square_y\,\frac{\delta}{\delta j_+(x)}\frac{\delta}{\delta j_-(y)}\,,\\[2ex] G^0_{+-}(x,y) \equiv \displaystyle\int\frac{d^3\boldsymbol{p}}{(2\pi)^3 2E_p}\,e^{ip\cdot(x-y)}\,.\end{cases}$$

An important point to keep in mind about Eq. (45) is that the external currents must be kept distinct in the amplitude and complex conjugate amplitude until all the derivatives contained in $\mathcal{D}$ have been taken. Only then one is allowed to set j_+ and j_- to the physical value of the external current. The propagator G^0_{+-}, that has only on-shell momentum modes, is the usual cut propagator that appears in *Cutkosky's cutting rules* [12,32]. The operator $\mathcal{D}$ acts on cut vacuum graphs by removing two sources (one on each side of the cut, *i.e.* a j_+ and a j_-), and by connecting the points where they were

[13] We are a bit careless here with the Lorentz indices, polarization vectors, *etc.*, because our main goal is to highlight the general techniques for keeping track of the diagrams that contribute to particle production in the saturated regime.

attached by the cut propagator G^0_{+-}. In fact, since P_n is obtained by acting n times with the operator $\mathcal{D}$, it is the sum of all the cut vacuum diagrams in which exactly n propagators are cut. Eq. (45) also makes obvious the fact that the probabilities P_n do not have a meaningful perturbative expansion in the saturated regime, because the sum $iV[j]$ of the connected vacuum diagrams starts at the order g^{-2}.

By summing Eq. (45) from $n = 0$ to ∞ while keeping j_+ and j_- distinct, one obtains the sum of all the cut vacuum diagrams with the current j_+ in the amplitude and j_- in the complex conjugate amplitude to be

$$\sum \begin{pmatrix} \text{all the cut} \\ \text{vacuum diagrams} \end{pmatrix} = e^{\mathcal{D}}\, e^{iV[j_+]}\, e^{-iV^*[j_-]}\,. \tag{46}$$

When we set $j_+ = j_-$, this sum becomes $\sum_n P_n$, and therefore it should be equal to 1 because of unitarity. Eq. (45) is very useful, because it allows to replace infinite sets of Feynman diagrams by simple algebraic equations. Similarly, the fact that Eq. (46) is 1 when $j_+ = j_-$ corresponds to a cancellation of an infinite set of graphs[14], that would be very difficult to see at the level of diagrams.

4.3. Inclusive gluon spectrum

Eq. (45) leads to compact formulas for moments of the distribution of produced particles. The first moment — the average multiplicity — reads [29]

$$\overline{N} = \sum_{n=0}^{\infty} n\, P_n = \mathcal{D}\left\{ e^{\mathcal{D}}\, e^{iV[j_+]}\, e^{-iV^*[j_-]} \right\}_{j_+=j_-=j}\,. \tag{47}$$

With the help of Eq. (46), this formula tells us that $\overline{N}$ is given by the action of the operator $\mathcal{D}$ on the sum of all the cut vacuum diagrams. In plain English, this translates into: take a cut vacuum diagram (connected or not), remove a source on each side of the cut, and put a cut propagator where the sources were attached. Depending on whether the cut vacuum diagram one starts from is connected or not, one gets two different topologies, displayed in figure 10. Each of the blobs in these diagrams can be any connected graph, and must be cut in all the possible ways[15]. Thus, only connected graphs contribute to the multiplicity.

[14] This cancellation is closely related to the *Abramovsky–Gribov–Kancheli cancellation* [33].

[15] Note that by not performing the $d^3\boldsymbol{p}$ integration contained in the explicit cut propagator, one obtains the *inclusive gluon spectrum* $d\overline{N}/d^3\boldsymbol{p}$ instead of the integrated multiplicity.

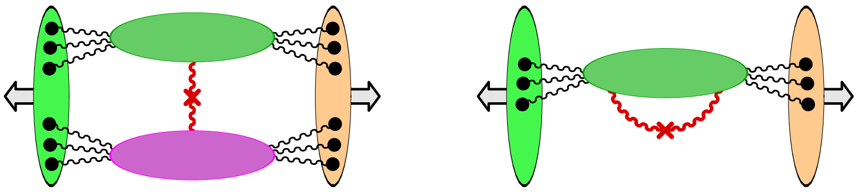

Fig. 10. The two topologies contributing to the average gluon multiplicity $\overline{N}$. In each blob, one must sum over all the possible ways of cutting the propagators.

An important point is that, even though the perturbative expansion for the P_n is not well defined, the multiplicity (and more generally any moment of the distribution P_n) can be organized in a sensible perturbative series[16]. The Leading Order is obtained by keeping only the leading order vacuum graphs, *i.e.* those that have no loops:

$$\overline{N}_{\rm LO} = \sum_{\rm trees} \sum_{\rm cuts} \tag{48}$$

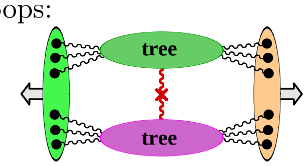

Thus $\overline{N}$ starts at the order g^{-2}. In Eq. (48), for each tree diagram, one must sum over all the possible ways of cutting its lines. The simplest way of doing this is to use Cutkosky's rules:

- assign $+$ or $-$ labels to each vertex and source of the graph, in all the possible ways (there are 2^n terms for a graphs with n vertices and sources). A $+$ vertex has a coupling $-ig$ and a $-$ vertex has a coupling $+ig$,
- the propagators depend on which type of labels they connect. In momentum space, they read:

$$\begin{aligned}
&G^0_{++}(p) = i/(p^2+i\epsilon) && \text{(standard Feynman propagator)}\\
&G^0_{--}(p) = -i/(p^2-i\epsilon) && \text{(complex conjugate of } G^0_{++}(p))\\
&G^0_{+-}(p) = 2\pi\theta(-p^0)\delta(p^2)\,, && G^0_{-+}(p) = 2\pi\theta(p^0)\delta(p^2)\,.
\end{aligned} \tag{49}$$

A quick analysis shows that, when one sets $j_+ = j_-$, summing over the $\pm$ labels at each vertex produces combinations of propagators,

$$G^0_{++}(p) - G^0_{+-}(p) = G^0_{\rm R}(p)\,, \quad G^0_{-+}(p) - G^0_{--}(p) = G^0_{\rm R}(p)\,, \tag{50}$$

[16] The fact that this is possible for $\overline{N}$ but not for the P_n's themselves is due to the fact that the only graphs that contribute to $\overline{N}$ are connected. This is a consequence of the AGK cancellation.

where $G^0_{\rm R}(p)$ is the *retarded propagator*[17]. Thus, for a given tree graph, doing the sum over the cuts simply amounts to replacing all its propagators by retarded propagators. The last step is to perform the sum over all the trees. It is a well known result that the sum of all the tree diagrams that end at a point x is a solution of the classical equations of motion of the field theory under consideration. In our case, this sum is a color field $\mathcal{A}^\mu(x)$ that obeys the Yang–Mills equations

$$[\mathcal{D}_\mu, \mathcal{F}^{\mu\nu}] = J^\nu\,, \tag{51}$$

where J^ν is the color current associated to the sources $\rho_{1,2}$ that represent the incoming projectiles (see Eq. (41)). The boundary conditions obeyed by $\mathcal{A}^\mu(x)$ depend on the nature of the propagators that entered in the sum of tree diagrams. When these propagators are all retarded, one gets a retarded solution of the Yang–Mills equations, that vanishes in the remote past, $\lim_{x_0\to-\infty}\mathcal{A}^\mu(x) = 0$. The precise formula for the gluon spectrum in terms of this solution of the Yang–Mills equations reads

$$\frac{d\overline{N}_{\rm LO}}{dY\,d^2\boldsymbol{p}_\perp} = \frac{1}{16\pi^3}\int d^4x d^4y\, e^{ip\cdot(x-y)}\,\Box_x\Box_y \sum_\lambda \epsilon^\mu_\lambda \epsilon^\nu_\lambda\; \mathcal{A}_\mu(x)\mathcal{A}_\nu(y)\,. \tag{52}$$

Solving the Yang–Mills equations is an easy problem in the case of a single source ρ, but turns out to be very challenging when there are two sources moving in opposite directions. The Schwinger gauge, defined by the constraint $\mathcal{A}^\tau \equiv x^+\mathcal{A}^- + x^-\mathcal{A}^- = 0$, is quite useful because it alleviates the need to ensure that the current J^ν is covariantly conserved[18]. In this gauge, $\mathcal{A}^+ = 0$ where $J^- \neq 0$ and conversely, which makes this condition trivial. Moreover, in this gauge, one can find the value of the gauge field on a time-like surface just above the light-cone (at a proper time $\tau = 0^+$) simply by matching the singularities across the light-cone. These initial conditions [34] can be written as[19]

$$\begin{aligned}
\mathcal{A}^i(\tau=0,\boldsymbol{x}_\perp) &= \mathcal{A}^i_1(\boldsymbol{x}_\perp) + \mathcal{A}^i_2(\boldsymbol{x}_\perp)\,,\\
\mathcal{A}^\eta(\tau=0,\boldsymbol{x}_\perp) &= -\frac{ig}{2}\left[\mathcal{A}^i_1(\boldsymbol{x}_\perp)\,,\,\mathcal{A}^i_2(\boldsymbol{x}_\perp)\right]\,,\\
\mathcal{A}^\tau &= 0\quad\text{(gauge condition)}\,,
\end{aligned} \tag{53}$$

[17] In momentum space, $G^0_{\rm R}(p) = i/(p^2 + i\,{\rm sign}(p_0)\,\epsilon)$. Therefore, in coordinate space, it is proportional to $\theta(x^0 - y^0)$, hence its name.

[18] In general gauges, one has to enforce the condition $\left[\mathcal{D}_\mu, J^\mu\right] = 0$ (this is a consequence of Jacobi's identity for commutators). Because this relation involves a covariant derivative rather than an ordinary derivative, the radiated field leads to modifications of the current itself.

[19] An interesting feature of the gauge fields at early times after the collision — a phase recently named "glasma" — is that the chromo-electric and magnetic fields are purely longitudinal, while they were transverse to the beam axis just before the collision [35].

where $\mathcal{A}^\eta \equiv \tau^{-2}(x^-\mathcal{A}^+ - x^=\mathcal{A}^-)$. In this formula, $\mathcal{A}_1^i(\boldsymbol{x}_\perp)$ and $\mathcal{A}_2^i(\boldsymbol{x}_\perp)$ are the gauge fields created by each nucleus [20] below the light-cone:

$$\begin{aligned}\mathcal{A}_1^i &= \frac{i}{g}U_1(\boldsymbol{x}_\perp)\partial^i U_1^\dagger(\boldsymbol{x}_\perp)\,,\; U_1(\boldsymbol{x}_\perp) = T_+ \exp ig\int dx^+ T^a \frac{1}{\boldsymbol{\nabla}_\perp^2}\rho_1^a(x^+,\boldsymbol{x}_\perp)\,,\\ \mathcal{A}_2^i &= \frac{i}{g}U_2(\boldsymbol{x}_\perp)\partial^i U_2^\dagger(\boldsymbol{x}_\perp)\,,\; U_2(\boldsymbol{x}_\perp) = T_- \exp ig\int dx^- T^a \frac{1}{\boldsymbol{\nabla}_\perp^2}\rho_2^a(x^-,\boldsymbol{x}_\perp)\,.\end{aligned} \tag{54}$$

Therefore, the problem of solving the Yang–Mills equations from $x_0 = -\infty$ to $x_0 = +\infty$ is reduced to solving them in the forward light-cone from a known initial condition[21].

Since our problem is invariant under boosts in the z direction, one can completely eliminate the space-time rapidity η from the equations of motion (and the initial conditions in Eq. (53) are also η-independent). Thus, in the forward light-cone, one has to solve numerically [36] equations of motion in time and two spatial dimensions, and then to evaluate Eq. (52). The result of this computation is displayed in figure 11. In this computation, the MV

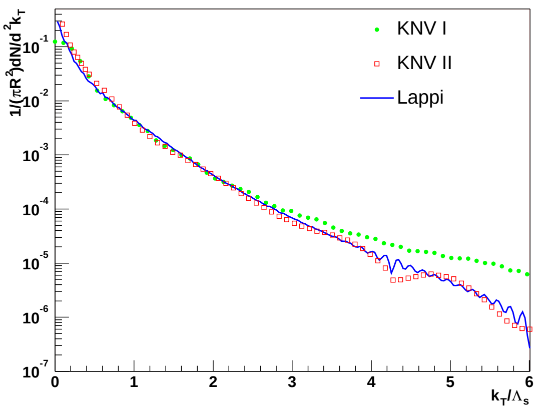

Fig. 11. The gluon spectrum at leading order in the CGC framework.

model was used as the distribution of the sources ρ_1 and ρ_2. Therefore, the dependence of the spectrum on the momentum rapidity Y of the produced gluon cannot be obtained in this calculation, and only the $k_\perp$ dependence is shown. The main effect of gluon recombinations on this spectrum is that it reduces the yield at low transverse momentum, $k_\perp \lesssim Q_\mathrm{s}$. Indeed, in

[20] Because retarded solutions are causal, the field below the light-cone cannot depend simultaneously on ρ_1 and ρ_2.

[21] At $\tau > 0$, the YM equations are the vacuum ones, since all the sources are on the light-cone.

a fixed order calculation in perturbative QCD, the spectrum would behave as $k_\perp^{-4}$. In the CGC picture, the singularity of the spectrum at low $k_\perp$ is only logarithmic[22], and is therefore integrable.

Note that a similar study has also been performed for the initial production of quarks in nucleus–nucleus collisions [37]. The inclusive quark spectrum can be calculated by solving the Dirac equation on top of the classical field $\mathcal{A}$, also with retarded boundary conditions.

4.4. Loop corrections to the gluon spectrum

The only quantities that have been evaluated in this framework so far are the gluon and the quark spectra, both at leading order. However, we *a priori* know what diagrams contribute to the gluon and quark multiplicities to all orders. There is therefore a well defined and systematic procedure to compute corrections to the previous results. Loop corrections to gluon production are very relevant for the following reasons:

- They contain terms that are divergent due to unbounded integrals over longitudinal momenta, very similar to the divergences encountered in the derivation of the BK equation. One should verify whether these divergences can be absorbed in the distributions $W[\rho_1]$ and $W[\rho_2]$ of the color sources of each projectile. This *factorization* is crucial for the internal consistency of the CGC framework.

- It has been noted recently that the boost invariant solution $\mathcal{A}^\mu(x)$ of the Yang–Mills equations is unstable[23]; rapidity dependent perturbations to this solution grow exponentially in time. Loop corrections generate this kind of rapidity dependent perturbations. Tracking all these terms and resumming them is very important in order to get meaningful answers from the CGC regarding the momentum distribution of the produced gluons, and may be relevant in the problem of thermalization in heavy ion collisions.

Note that these two items address very different stages of the collision process. The first relates to the incoming wavefunctions (and as such should be independent of the subsequent collision), while the second issue is about what happens in the final state after the collision. Therefore, we should aim at writing the 1-loop corrections in a way that separates the initial and final state as clearly as possible.

[22] If the final Fourier decomposition is performed at a finite time τ, the spectrum is completely regular when $k_\perp \to 0$.

[23] This instability is very similar to the Weibel instability that occurs in anisotropic plasmas [40, 41].

Let us start by listing the relevant diagrams: the 1-loop corrections to the average multiplicity are shown in the diagrams of figure 12. The topology

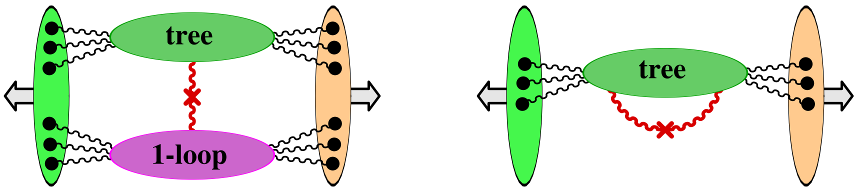

Fig. 12. 1-loop diagrams contributing to the gluon spectrum.

on the left is very similar to the one already encountered at tree level, except that one of the blobs has now a loop correction in it. The topology on the right is new; but it is in fact similar to what we had to evaluate in the case of the quark spectrum [37,38], except that the quark loop must be replaced by a gluon loop. The NLO contribution to the gluon spectrum can be written as

$$\frac{d\overline{N}_{\rm NLO}}{dY d^2\boldsymbol{p}_\perp} = \frac{1}{16\pi^3}\int d^4x d^4y\, e^{ip\cdot(x-y)}\,\square_x\square_y\sum_\lambda \epsilon^\lambda_\mu\epsilon^\lambda_\nu\Big[\mathcal{A}^\mu(x)\delta\mathcal{A}^\nu(y)$$
$$+\delta\mathcal{A}^\mu(x)\mathcal{A}^\nu(y)+G^{\mu\nu}_{+-}(x,y)\Big]\,. \tag{55}$$

The first two terms are the contribution of the diagram on the left of figure 12 (the loop can be in either of the two blobs), and the last term on the second line comes from the diagram on the right. The field $\delta\mathcal{A}$ that appears on the first line is the 1-loop correction to $\mathcal{A}$; and it obeys the linearized equation of motion for small fluctuations. $G^{\mu\nu}_{+-}$ is the cut propagator of a gluon, with the classical field $\mathcal{A}$ in the background.

Let us now illustrate how one can separate the initial state from the final state in the term that contains $G^{\mu\nu}_{+-}(x,y)$. First, by analogy with the case of quark production [37], we can write

$$\int d^4xd^4ye^{ip\cdot(x-y)}\square_x\square_y\sum_\lambda\epsilon^\lambda_\mu\epsilon^\lambda_\nu\, G^{\mu\nu}_{+-}(x,y) = \sum_{\lambda,\lambda'}\int\frac{d^3\boldsymbol{q}}{(2\pi)^3 2E_{\boldsymbol{q}}}\left|\mathcal{T}^{\lambda\lambda'}_{\rm R}(\boldsymbol{p},\boldsymbol{q})\right|^2,$$
$$\mathcal{T}^{\lambda\lambda'}_{\rm R}(\boldsymbol{p},\boldsymbol{q}) \equiv \lim_{x_0\to+\infty}\int d^3\boldsymbol{x}\, e^{ip\cdot x}\,(\partial^0_x - iE_{\boldsymbol{p}})\,\epsilon^\lambda_\mu\, a^\mu_{\lambda'\boldsymbol{q}}(x)\,, \tag{56}$$

where $a^\mu_{\lambda'\boldsymbol{q}}(x)$ is a small fluctuation of the gauge field on top of $\mathcal{A}^\mu$, with initial condition $\epsilon^\mu_{\lambda'}e^{iq\cdot x}$ when $x_0\to-\infty$. The equation of motion of this fluctuation is obtained by writing the Yang–Mills equations for $\mathcal{A}+a$ and by linearizing it in a. A central formula in order to separate the initial and final states is the following[24]

$$a(x) = \int\limits_{\tau=0^+} d^3\boldsymbol{y}\, \Big[a(0,\boldsymbol{y})\cdot \boldsymbol{T_y}\Big]\, \mathcal{A}(x)\,, \tag{57}$$

where $(0,\boldsymbol{y})$ denotes a point located on the light-cone ($\tau=0$) ($\boldsymbol{y}$ represents any set of three coordinates that map the light-cone) and where $\boldsymbol{T_y}$ is the generator of translations of the initial fields at the point $\boldsymbol{y}$ on the light-cone. In this formula, the classical field $\mathcal{A}$ is considered as a functional of its initial condition $\mathcal{A}(0,\boldsymbol{y})$ on the light-cone. The proof of Eq. (57) is straightforward[25], but its diagrammatic interpretation is more interesting. Note first that $\mathcal{A}^\mu(x)$, seen as a functional of its initial condition on the light-cone, can also be represented by tree diagrams, as illustrated in the left panel of figure 13. (This can be seen from the Green's formula for $\mathcal{A}(x)$.) The action of the operator $\boldsymbol{T_y}$ on the classical field $\mathcal{A}(x)$ is to replace one of the

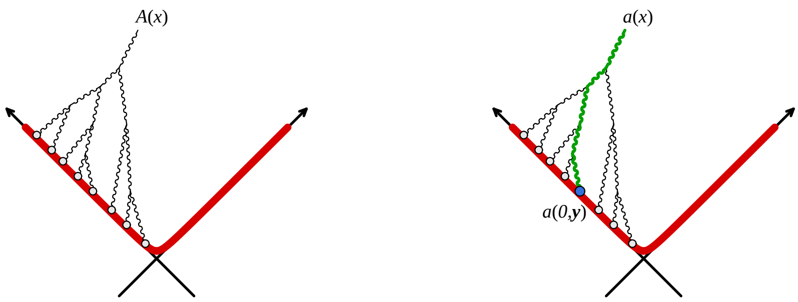

Fig. 13. Left: diagrammatic representation of $\mathcal{A}$ as a function of its initial condition on the light-cone (the open dots represent the initial $\mathcal{A}(0,\boldsymbol{y})$). Right: propagation of a small fluctuation on top of the classical field.

open dots in figure 13 by the fluctuation $a(0,\boldsymbol{y})$, represented by a filled dot in the right panel of figure 13. The diagram one gets after this is nothing but a contribution to the propagation of a small fluctuation over the classical

[24] To avoid encumbering the equations with indices of various kinds, we are suppressing all the indices in this and the following formula.

[25] Write the Green's formula that expresses $\mathcal{A}(x)$ in terms of the initial $\mathcal{A}(0,\boldsymbol{y})$, insert it in Eq. (57), and check that this leads to the Green's formula that relates $a(x)$ to its initial condition $a(0,\boldsymbol{y})$.

field. Plugging Eq. (57) in Eq. (56), this quantity becomes

$$\begin{aligned}
&\lim_{x_0=y_0\to+\infty}\int d^3\boldsymbol{x}d^3\boldsymbol{y}\,e^{ip\cdot(x-y)}\,(\partial_x^0-iE_{\boldsymbol{p}})(\partial_y^0+iE\boldsymbol{p})\sum_\lambda\epsilon_\mu^\lambda\epsilon_\nu^\lambda\\
&\times\int\limits_{\tau=0^+}d^3\boldsymbol{u}d^3\boldsymbol{v}\sum_{\lambda'}\int\frac{d^3\boldsymbol{q}}{(2\pi)^3 2E_{\boldsymbol{q}}}\\
&\times\left[\left[a_{\lambda'\boldsymbol{q}}(0,\boldsymbol{u})\cdot\boldsymbol{T_u}\right]\mathcal{A}^\mu(x)\right]\left[\left[a^*_{\lambda'\boldsymbol{q}}(0,\boldsymbol{v})\cdot\boldsymbol{T_v}\right]\mathcal{A}^\nu(y)\right]. \qquad (58)
\end{aligned}$$

The brackets are crucial in this formula, in order to limit the scope of the derivatives contained in the operators $\boldsymbol{T_u}$ and $\boldsymbol{T_v}$. Note that, if it were not for these brackets, the first line and the two $\mathcal{A}$'s of the second line would be nothing but the LO gluon spectrum. It turns out that, after one adds the first two in Eq. (55), the NLO correction to the spectrum can be written as

$$\begin{aligned}
\frac{d\overline{N}_{\rm NLO}}{dYd^2\boldsymbol{p}_\perp} = &\Bigg[\int\limits_{\tau=0^+}d^3\boldsymbol{u}\left[\delta\mathcal{A}(0,\boldsymbol{u})\cdot\boldsymbol{T_u}\right]\\
&+\int\limits_{\tau=0^+}d^3\boldsymbol{u}d^3\boldsymbol{v}\left[\varSigma(\boldsymbol{u},\boldsymbol{v})\cdot\boldsymbol{T_u}\boldsymbol{T_v}\right]\Bigg]\frac{d\overline{N}_{\rm LO}}{dYd^2\boldsymbol{p}_\perp}, \qquad (59)
\end{aligned}$$

where the LO spectrum is considered as a functional of the initial classical field on the light-cone. In this equation, $\delta\mathcal{A}(0,\boldsymbol{u})$ is the value of $\delta\mathcal{A}$ on the light-cone, and the 2-point $\varSigma(\boldsymbol{u},\boldsymbol{v})$ is defined as

$$\varSigma(\boldsymbol{u},\boldsymbol{v})\equiv\frac{1}{2}\sum_{\lambda'}\int\frac{d^3\boldsymbol{q}}{(2\pi)^3 2E_{\boldsymbol{q}}}\,a_{\lambda'\boldsymbol{q}}(0,\boldsymbol{u})a^*_{\lambda'\boldsymbol{q}}(0,\boldsymbol{v})\,. \qquad (60)$$

Note that $\delta\mathcal{A}(0,\boldsymbol{u})$ and $\varSigma(\boldsymbol{u},\boldsymbol{v})$ are in principle calculable analytically. Eq. (59) realizes the separation we were seeking of the initial and final states. Indeed, the operator in the square bracket depends only on what happens below the light-cone, *i.e.* before the collision. On the contrary, the LO spectrum seen as a functional of the initial classical field $\mathcal{A}$ depends only on the final state dynamics. The other benefit of this formula is that is expresses the NLO correction as a perturbation of the LO one; this property — that seems generalizable to other inclusive observables — suggests the universality of the initial state divergences and their factorizability.

From Eq. (59), it is easy to see that the coefficients $\delta\mathcal{A}(0,\boldsymbol{u})$ and $\varSigma(\boldsymbol{u},\boldsymbol{v})$ are formally infinite. For $\varSigma(\boldsymbol{u},\boldsymbol{v})$ for instance, the integration over the longitudinal component of the momentum $\boldsymbol{q}$ in Eq. (60) diverges. A similar divergence occurs in the loop contained in $\delta\mathcal{A}(0,\boldsymbol{u})$. The fact that these divergences arise in the first factor of Eq. (59) indicates that they are related to the evolution of the initial projectiles prior to the collision. These divergences can be momentarily regularized by introducing cutoffs Y_0, Y_0' in rapidity around the rapidity Y at which the spectrum is calculated. Thus, $\delta\mathcal{A}(0,\boldsymbol{u})$ and $\Sigma(\boldsymbol{u},\boldsymbol{v})$ become finite but depend on these unphysical cutoffs. To be consistent, the distribution of the sources ρ_1 and ρ_2 should be evolved from the beam rapidities to Y_0 and Y_0', respectively. Thus, the complete formula for the LO+NLO spectrum, including the average over the sources, should be

$$\frac{d\overline{N}_{\rm LO+NLO}}{dY\,d^2\boldsymbol{p}_\perp} = \int \big[D\rho_1\big]\big[D\rho_2\big]\, W_{Y_{\rm beam}-Y_0}[\rho_1] W_{Y_{\rm beam}+Y_0'}[\rho_2]$$
$$\times \underbrace{\left[1+\int\limits_{\tau=0^+} d^3\boldsymbol{u}\,\Big[\delta\mathcal{A}(0,\boldsymbol{u})\cdot\boldsymbol{T}_{\boldsymbol{u}}\Big]+\int\limits_{\tau=0^+} d^3\boldsymbol{u}d^3\boldsymbol{v}\,\Big[\Sigma(\boldsymbol{u},\boldsymbol{v})\cdot\boldsymbol{T}_{\boldsymbol{u}}\boldsymbol{T}_{\boldsymbol{v}}\Big]\right]_{Y_0'}^{Y_0}}_{\mathcal{O}^{Y_0}_{Y_0'}[\rho_1,\rho_2]} \frac{d\overline{N}_{\rm LO}}{dY\,d^2\boldsymbol{p}_\perp}\,, \tag{61}$$

where the subscript Y_0' and superscript Y_0 indicate that the momentum integrals contained in the bracket have cutoffs in rapidity. Recall that the LO spectrum in the right hand side is a function of $\mathcal{A}$ on the light-cone, which is itself a function of $\rho_{1,2}$. The factorizability of these divergences in the initial state is equivalent to the independence of the previous formula with respect to the unphysical Y_0 and Y_0'. Recent work indicates that

$$\frac{\partial\mathcal{O}^{Y_0}_{Y_0'}[\rho_1,\rho_2]}{\partial Y_0} = \mathcal{H}^\dagger[\rho_1]\,, \tag{62}$$

which is enough to ensure a cancellation of the leading Y_0 dependence. A similar relation holds, that eliminates the dependence on Y_0'.

Eq. (59) also allows us to discuss the issue of the instability of the boost invariant classical solution. These instabilities manifest themselves in the fact that the action of $\boldsymbol{T}_{\boldsymbol{u}}$ on $\mathcal{A}(x)$ diverges when the time x_0 goes to infinity. Indeed,

$$\boldsymbol{T}_{\boldsymbol{u}}\mathcal{A}(x) \sim \frac{\delta\mathcal{A}(x)}{\delta\mathcal{A}(0,\boldsymbol{y})} \tag{63}$$

is a measure of how $\mathcal{A}(x)$ is sensitive to its initial condition. Therefore, if the solution $\mathcal{A}(x)$ is unstable, small perturbations of its initial condition lead to exponentially growing changes in the solution. From the numerical study of these instabilities (see figure 14), one gets [40] $\boldsymbol{T}_{\boldsymbol{u}}\mathcal{A}(x) \sim e^{\sqrt{\mu\tau}}$, where μ is

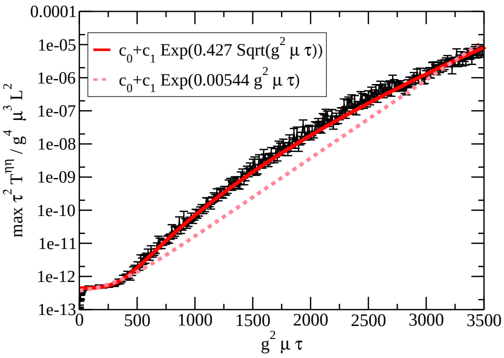

Fig. 14. Time dependence of small fluctuations on top of the boost independent classical field.

of the order of the saturation momentum. This means that, although the 1-loop corrections are suppressed by a factor α_s compared to the LO, some of these corrections are enhanced by factors that grow exponentially in time after the collision. At first sight, one may expect a complete breakdown of the CGC description at $\tau_{\max} \sim Q_s^{-1} \ln^2\left(\frac{1}{\alpha_s}\right)$, *i.e.* the time at which the 1-loop corrections become as large as the LO contribution. The only way out of this conclusion is to resum all these enhanced corrections in the hope that the resummed series is better behaved when $\tau \to +\infty$. Let us assume for the time being that we have performed this resummation, and that the sum of these enhanced terms generalize Eq. (59) to read

$$\frac{d\overline{N}_{\rm resummed}}{dY\,d^2\boldsymbol{p}_\perp} = Z[\boldsymbol{T_u}]\,\frac{d\overline{N}_{\rm LO}[\mathcal{A}(0,\boldsymbol{u})]}{dY\,d^2\boldsymbol{p}_\perp}\,, \tag{64}$$

where $Z[\boldsymbol{T_u}]$ is a certain functional of the operator $\boldsymbol{T_u}$. In the right hand side, we have emphasized the fact that the LO spectrum is a functional of the initial classical field on the light-cone. This formula can be written in a more intuitive way by performing a Fourier transform of $Z[\boldsymbol{T_u}]$,

$$Z[\boldsymbol{T_u}] \equiv \int \big[Da(\boldsymbol{u})\big]\, e^{i\int_{\tau=0^+} d^3\boldsymbol{u}\,\left[a(\boldsymbol{u})\cdot\boldsymbol{T_u}\right]}\, \widetilde{Z}[a(\boldsymbol{u})]\,. \tag{65}$$

In this formula, the functional integration $[Da(\boldsymbol{u})]$ is in fact an integration over two fields: the fluctuation $a(\boldsymbol{u})$ itself and its derivative normal to the light-cone $(n\cdot\partial_u)a(\boldsymbol{u})$. Thanks to the fact that $\boldsymbol{T_u}$ is the generator of translations of the initial conditions on the light-cone, the exponential in the previous formula is the translation operator itself. Therefore, when this exponential acts on a functional of the initial classical field $\mathcal{A}(0,\boldsymbol{u})$, it gives the same functional evaluated with a shifted initial condition $\mathcal{A}(0,\boldsymbol{u})+a(\boldsymbol{u})$. Therefore, we can write

$$\frac{d\overline{N}_{\rm resummed}}{dY d^2\boldsymbol{p}_\perp} = \int \big[Da(\boldsymbol{u})\big]\, \widetilde{Z}[a(\boldsymbol{u})]\, \frac{d\overline{N}_{\rm LO}[\mathcal{A}(0,\boldsymbol{u})+a(\boldsymbol{u})]}{dY d^2\boldsymbol{p}_\perp}\,. \tag{66}$$

We see that the effect of the resummation is simply to add fluctuations to the initial conditions of the classical field, with a distribution that depends on the details of the resummation[26]. It is easy to understand why these fluctuations are crucial in the presence of instabilities: despite the fact that they are suppressed by an extra power of $\alpha_{\rm s}$, the instabilities make them grow and eventually become as large as the LO. One can also see that the resummation has the effect of lifting the time limitation $\tau \le \tau_{\rm max}$. Indeed, after the resummation, the fluctuation $a(\boldsymbol{u})$ has entered in the initial condition for the full Yang–Mills equation, whose non-linearities prevent the solution from blowing up. A very important question is whether these instabilities fasten the local thermalization of the system formed in heavy ion collisions.

4.5. Summary and outlook

If the initial state factorization works as expected, and after the resummation of the leading contributions of the instability, the formula for the gluon spectrum should read

$$\begin{aligned}\frac{d\overline{N}}{dY d^2\boldsymbol{p}_\perp} &= \int \big[D\rho_1\big]\big[D\rho_2\big]\; W_{Y_{\rm beam}-Y}[\rho_1]\, W_{Y_{\rm beam}+Y}[\rho_2] \\ &\quad\times \int \big[Da\big]\, \widetilde{Z}[a]\, \frac{d\overline{N}_{\rm LO}[\mathcal{A}(0,\boldsymbol{u})+a(\boldsymbol{u})]}{dY d^2\boldsymbol{p}_\perp}\,. \end{aligned} \tag{67}$$

This formula resums the most singular terms at each order in $\alpha_{\rm s}$. Because of their relation to the physics of the initial and final state, respectively, the distributions $W[\rho]$ generalize parton distributions, while $\widetilde{Z}[a]$ plays a role similar to that of a fragmentation function[27].

Note that, even after the resummations performed in the initial and final states of Eq. (67), this formula still suffers from the usual problem of collinear gluon splitting in the final state. This is not a serious concern in heavy ion collisions though, because collinear singularities occur only when one takes the $\tau \to +\infty$ limit, and we do expect to have to switch to another description (like hydrodynamics) long before this becomes a problem. In

[26] In a recent work by one of the authors, using a completely different approach, the spectrum of initial fluctuations was found to be Gaussian [42].

[27] Naturally, this function has nothing to do with a gluon fragmenting into a hadron. Instead, it is related to how classical fields become gluons.

fact, the initial condition for hydrodynamics should be specified in terms of the energy-momentum tensor, which is infrared and collinear safe because it measures only the flow of energy and momentum.

A more important problem, that has still not received a satisfactory answer, is to understand how the initial particle spectrum — or the local energy momentum-tensor — reaches a state of local thermal equilibrium.

I would like to thank the organizers of the school — and in particular C. Royon — for their invitation to present these lectures, and for their efforts in creating an enjoyable and stimulating atmosphere. This work is supported in part by Agence Nationale de la Recherche via the programme ANR-06-BLAN-0285-01.

REFERENCES

[1] D.J. Gross, F. Wilczek, *Phys. Rev. Lett.* **30**, 1343 (1973); *Phys. Rev.* **D8**, 3633 (1973); *Phys. Rev.* **D9**, 980 (1974); H.D. Politzer, *Phys. Rev. Lett.* **30**, 1346 (1973); *Phys. Rep.* **14**, 129 (1974).

[2] S. Catani, M. Ciafaloni, F. Hautmann, *Nucl. Phys.* **B366**, 135 (1991); J.C. Collins, R.K. Ellis, *Nucl. Phys.* **B360**, 3 (1991).

[3] J.C. Collins, D.E. Soper, G. Sterman, *Nucl. Phys.* **B250**, 199 (1985); *Nucl. Phys.* **B261**, 104 (1985); *Nucl. Phys.* **B263**, 37 (1986).

[4] E.A. Kuraev, L.N. Lipatov, V.S. Fadin, *Sov. Phys. JETP* **45**, 199 (1977); I. Balitsky, L.N. Lipatov, *Sov. J. Nucl. Phys.* **28**, 822 (1978).

[5] V.N. Gribov, L.N. Lipatov, *Sov. J. Nucl. Phys.* **15**, 438 (1972); *Sov. J. Nucl. Phys.* **15**, 675 (1972); Yu. Dokshitzer, *Sov. Phys. JETP* **46**, 641 (1977); G. Altarelli, G. Parisi, *Nucl. Phys.* **B126**, 298 (1977).

[6] S.D. Drell, J.D. Walecka, *Ann. Phys.* **28**, 18 (1964).

[7] E.D. Bloom *et al.*, *Phys. Rev. Lett.* **23**, 930 (1969); M. Breidenbach *et al.*, *Phys. Rev. Lett.* **23**, 935 (1969).

[8] J.D. Bjorken, *Phys. Rev.* **148**, 1467 (1966); SLAC-PUB-0571 (1969).

[9] C.G. Callan, D.J. Gross, *Phys. Rev. Lett.* **22**, 156 (1969).

[10] R.P. Feynman, *Photon–Hadron Interactions, Frontiers in Physics*, W.A. Benjamin, 1972; J.D. Bjorken, *Lect. Notes Phys.*, **56**, Springer, Berlin 1976.

[11] K.G. Wilson, *Phys. Rev.* **179**, 1499 (1969).

[12] M.E. Peskin, D.V. Schroeder, *An Introduction to Quantum Field Theory*, Addison-Wesley, New York 1995.

[13] J. Gayler [H1 and ZEUS Collaborations], `hep-ex/0603037`.

[14] J.D. Bjorken, J.B. Kogut, D.E. Soper, *Phys. Rev.* **D3**, 1382 (1971).

[15] H. Weigert, *Nucl. Phys.* **A703**, 823 (2002).

[16] Yu.V. Kovchegov, *Phys. Rev.* **D60**, 034008 (1999).

[17] Yu.V. Kovchegov, *Phys. Rev.* **D61**, 074018 (2000).

[18] I. Balitsky, *Nucl. Phys.* **B463**, 99 (1996).

[19] A.H. Mueller, *Phys. Lett.* **B523**, 243 (2001).

[20] L.V. Gribov, E.M. Levin, M.G. Ryskin, *Phys. Rep.* **100**, 1 (1983); A.H. Mueller, J.-W. Qiu, *Nucl. Phys.* **B268**, 427 (1986); J.P. Blaizot, A.H. Mueller, *Nucl. Phys.* **B289**, 847 (1987).

[21] L.D. McLerran, R. Venugopalan, *Phys. Rev.* **D49**, 2233 (1994); *Phys. Rev.* **D49**, 3352 (1994); *Phys. Rev.* **D50**, 2225 (1994).

[22] J. Jalilian-Marian, A. Kovner, L.D. McLerran, H. Weigert, *Phys. Rev.* **D55**, 5414 (1997); J. Jalilian-Marian, A. Kovner, A. Leonidov, H. Weigert, *Nucl. Phys.* **B504**, 415 (1997); *Phys. Rev.* **D59**, 014014, 034007, Erratum, 099903 (1999); E. Iancu, A. Leonidov, L.D. McLerran, *Nucl. Phys.* **A692**, 583 (2001); *Phys. Lett.* **B510**, 133 (2001); E. Ferreiro, E. Iancu, A. Leonidov, L.D. McLerran, *Nucl. Phys.* **A703**, 489 (2002).

[23] Yu.V. Kovchegov, *Phys. Rev.* **D54**, 5463 (1996).

[24] S. Jeon, R. Venugopalan, *Phys. Rev.* **D70**, 105012 (2004); *Phys. Rev.* **71**, 125003 (2005).

[25] S. Munier, R. Peschanski, *Phys. Rev. Lett.* **91**, 232001 (2003); *Phys. Rev.* **D69**, 034008 (2004); *Phys. Rev.* **D70**, 077503 (2004).

[26] A.M. Stasto, K. Golec-Biernat, J. Kwiecinski, *Phys. Rev. Lett.* **86**, 596 (2001); E. Iancu, K. Itakura, L.D. McLerran, *Nucl. Phys.* **A708**, 327 (2002); C. Marquet, L. Schoeffel, *Phys. Lett.* **B639**, 471 (2006); F. Gelis, R. Peschanski, L. Schoeffel, G. Soyez, *Phys. Lett.* **B647**, 376 (2007).

[27] K. Golec-Biernat, M. Wusthoff, *Phys. Rev.* **D59**, 014017 (1999); *Phys. Rev.* **D60**, 114023 (1999); J. Bartels, K. Golec-Biernat, H. Kowalski, *Phys. Rev.* **D66**, 014001 (2002); E. Iancu, K. Itakura, S. Munier, *Phys. Lett.* **B590**, 199 (2004).

[28] Yu.V. Kovchegov, A.H. Mueller, *Nucl. Phys.* **B529**, 451 (1998); A. Kovner, U. Wiedemann, *Phys. Rev.* **D64**, 114002 (2001); Yu.V. Kovchegov, K. Tuchin, *Phys. Rev.* **D65**, 074026 (2002); A. Dumitru, L.D. McLerran, *Nucl. Phys.* **A700**, 492 (2002); A. Dumitru, J. Jalilian-Marian, *Phys. Rev. Lett.* **89**, 022301 (2002); *Phys. Lett.* **B547**, 15 (2002); F. Gelis, J. Jalilian-Marian, *Phys. Rev.* **D67**, 074019 (2003); J.P. Blaizot, F. Gelis, R. Venugopalan, *Nucl. Phys.* **A743**, 13, 57 (2004); F. Gelis, Y. Methar-Tani, *Phys. Rev.* **D73**, 034019 (2006); N.N. Nikolaev, W. Schafer, *Phys. Rev.* **D71**, 014023 (2005); J. Jalilian-Marian, Y. Kovchegov, *Prog. Part. Nucl. Phys.* **56**, 104 (2006); F. Gelis, J. Jalilian-Marian, *Phys. Rev.* **D66**, 014021, 094014 (2002); J. Jalilian-Marian, *Nucl. Phys.* **A753**, 307 (2005); F. Gelis, J. Jalilian-Marian, *Phys. Rev.* **D76**, 074015 (2007) [`hep-ph/0609066`].

[29] F. Gelis, R. Venugopalan, *Nucl. Phys.* **A776**, 135 (2006).

[30] F. Gelis, R. Venugopalan, *Nucl. Phys.* **A779**, 177 (2006).

[31] F. Gelis, R. Venugopalan, *Acta Phys. Pol. B* **37**, 3253 (2006), `hep-ph/0611157`.

[32] R.E. Cutkosky, *J. Math. Phys.* **1**, 429 (1960).

[33] V.A. Abramovsky, V.N. Gribov, O.V. Kancheli, *Sov. J. Nucl. Phys.* **18**, 308 (1974).

[34] A. Kovner, L.D. McLerran, H. Weigert, *Phys. Rev.* **D52**, 6231 (1995).

[35] T. Lappi, L.D. McLerran, *Nucl. Phys.* **A772**, 200 (2006).

[36] A. Krasnitz, R. Venugopalan, *Nucl. Phys.* **B557**, 237 (1999); *Phys. Rev. Lett.* **84**, 4309 (2000); *Phys. Rev. Lett.* **86**, 1717 (2001); A. Krasnitz, Y. Nara, R. Venugopalan, *Nucl. Phys.* **A727**, 427 (2003); *Phys. Rev. Lett.* **87**, 192302 (2001); T. Lappi, *Phys. Rev.* **C67**, 054903 (2003).

[37] F. Gelis, K. Kajantie, T. Lappi, *Phys. Rev.* **C71**, 024904 (2005); *Phys. Rev. Lett.* **96**, 032304 (2006).

[38] A.J. Baltz, F. Gelis, L.D. McLerran, A. Peshier, *Nucl. Phys.* **A695**, 395 (2001).

[39] F. Gelis, T. Lappi, R. Venugopalan, in preparation.

[40] P. Romatschke, R. Venugopalan, *Phys. Rev. Lett.* **96**, 062302 (2006); *Eur. Phys. J.* **A29**, 71 (2006); *Phys. Rev.* **D74**, 045011 (2006).

[41] S. Mrowczynski, *Phys. Lett.* **B214**, 587 (1988); *Phys. Lett.* **B314**, 118 (1993); *Phys. Lett.* **B363**, 26 (1997); S. Mrowczynski, M.H. Thoma, *Phys. Rev.* **D62**, 036011 (2000); A.K. Rebhan, P. Romatschke, M. Strickland, *Phys. Rev. Lett.* **94**, 102303 (2005); *J. High Energy Phys.* **0509**, 041 (2005); P. Arnold, J. Lenaghan, G.D. Moore, *J. High Energy Phys.* **0308**, 002 (2003); P. Arnold, J. Lenaghan, G.D. Moore, L.G. Yaffe, *Phys. Rev. Lett.* **94**, 072302 (2005).

[42] K. Fukushima, F. Gelis, L. McLerran, *Nucl. Phys.* **A786**, 107 (2007).

[43] F. Gelis, S. Jeon, R. Venugopalan, `arXiv:0706.3775 [hep-ph]`.